*Structure & Methods, ISBN 0-940030-32-2*
*Volume 3: DNA & RNA, ISBN 0-940030-31-4*
*Eds., Ramaswamy H. Sarma & Mukti H. Sarma,* © *Adenine Press 1990*

# Parallel Stranded DNA

**Thomas M. Jovin, Karsten Rippe, Niels B. Ramsing, Reinhard Klement, Wim Elhorst and Marie Vojtišková**
Department of Molecular Biology
Max Planck Institute for Biophysical Chemistry
Postfach 2841, D-3400 Göttingen, FRG

***Abstract***

Two DNA oligonucleotides consisting of dA and dT residues in sequences with complementarity in a parallel orientation can hybridize spontaneously, forming a duplex structure distinctly different from that of the conventional antiparallel B-DNA helix. The helical stability and other features of this parallel stranded DNA conformation (ps-DNA) have been determined with a series of linear duplexes 15 to 25-nt in length as well as with specially designed hairpin molecules. Ps-DNA is characterized by the following properties: (i) *Spectra*. The UV absorption is blue shifted relative to that of B-DNA (aps-DNA) such that the difference spectra (ps -aps) in the native state show a positive peak (~ 250 nm) in the region of 235-265 nm, an isosbestic point at 267 nm, and a negative peak (~ 280 nm) in the range 270-300 nm. The CD and the $^{31}$P-NMR spectra of the native ps duplexes also differ significantly from those of their aps counterparts. (ii) *Helical stability*. The van't Hoff transition enthalpies $\Delta H_{vH}$ determined from temperature resolved UV absorption spectra are found to be independent of salt concentration, and are similar in magnitude for all related sets of molecules when expressed per nearest neighbor interaction (N.N. $\equiv (n-1)$ where $n$ is the chain length). That is, $\Delta H_{vH}$/N.N. = 20 ± 2 kJ mol$^{-1}$ for ps-DNA and 25 ± 2 kJ mol$^{-1}$ for aps-DNA in NaCl. The melting temperatures are 13-19° lower for the ps compared to the aps duplexes (10° in the case of the hairpins), but the $T_m$ values of all molecules show essentially the same dependence upon salt concentration. (iii) *Drug binding*. The intercalating drug ethidium bromide binds better to ps- than to aps-DNA, but the opposite is true of the minor groove specific drugs bis-benzimidazole H-33258 (BBI-258) and 4′,6-diamidine-2-phenylindol (DAPI). (iv) *Substrate specificities*. The spectrum of reactivity of ps duplexes as substrates for DNA specific enzymes and chemical reagents is broad, ranging from a total lack of reaction to greater susceptibility relative to that of the corresponding aps molecules. (v) *Influence of dG · dC base pairs*. The substitution of four dA · dT base pairs with dG · dC base pairs in a 25-nt duplex destabilizes but does not abolish the ps conformation. (vi) *Model calculations*. Force field calculations yield models for the ps-DNA helix and the constituent *trans* base pairs.

## *Introduction*

In 1986, N. Pattabiraman (1) reported force field calculations predicting a stable homopolymeric duplex $d(A)_6 \cdot d(T)_6$ with the two strands oriented in the same 5′-3′ direction. The secondary structure of the proposed parallel stranded helix was

characterized by *reverse* Watson-Crick base pairing; i.e., a *trans* orientation of the glycosidic bonds of the dA and dT hydrogen bonded residues, denoted here as *trans*-Crick-Watson base pairs. Furthermore, the predicted helical stability was comparable to that of the corresponding antiparallel B-DNA structure.

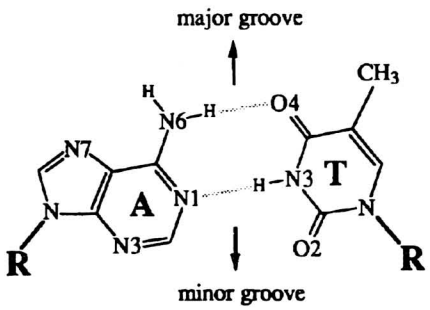


*cis*-Watson-Crick base pair

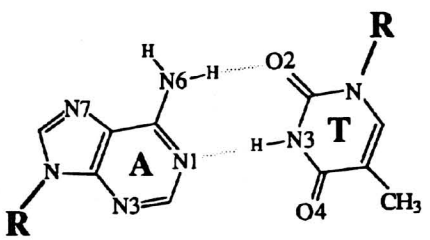


*trans*-Crick-Watson base pair

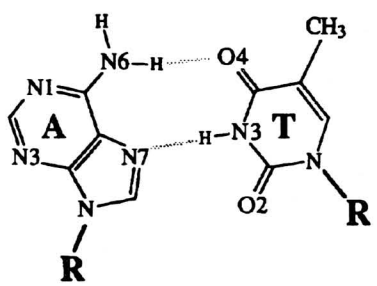


Hoogsteen base pair

The first experimental demonstration of parallel stranded DNA (ps-DNA) was with a series of hairpin molecules (Figure 1A) in which 3′-p-3′ and 5′-p-5′ phosphodiester bonds were introduced in the loops consisting of four dC nucleotides (hairpin ps-C10) or four dG nucleotides (hairpin ps-G10), thereby forcing the strands of $d(A)_{10} \cdot d(T)_{10}$ stems into a parallel orientation (2). Studies of these molecules demonstrated that (i) the ps hairpins are only slightly less stable than reference aps molecules, and that (ii) they exhibit characteristic differences in absorption and CD spectra, electrophoretic mobilities, enzyme substrate specificities, and drug-binding properties (2). The existence of Hoogsteen base pairing (see above) observed with other DNA structures involving parallel stranded interactions was excluded on the basis of the chemical methylation pattern obtained with dimethyl sulfate (2).

The findings with ps hairpins stimulated further studies with linear duplexes of oligonucleotides. The construction of ps linear duplexes requires selection of sequences for which the parallel orientation with perfect complementarity is greatly favored over alternative antiparallel secondary structures. A set of three 21-nt deoxyo-

ligonucleotides ("C-series," see Figure 1B) was devised according to these criteria and provided the first evidence for a ps-DNA duplex arising from the spontaneous hybridization of two strands (3); a somewhat different approach was reported by Germann *et al.* (4). The selection rules discriminating against competitive antiparallel structures were refined and led to the design and synthesis of four 25-nt deoxyoligonucleotides ("D-series," see Figure 1C) (5). The ps duplexes in both the C- and the D-series showed a 1:1 strand stoichiometry and exhibited spectroscopic, thermodynamic, electrophoretic, and ligand binding properties (3,5,6) different from the aps references but comparable to those obtained previously with the hairpin molecules.

More recently, other studies have been carried out with the D-series duplexes. They have been evaluated as substrates for a number of DNA dependent enzymes and chemical nucleases (7) and $^{31}$P-NMR spectra have been obtained (K. Rippe, N.B. Ramsing, F. Eckstein and T.M. Jovin, in preparation). In addition, we have constructed variants of the D-series in which four dA residues in one strand and the dT residues in the complementary strand have been replaced with dG and dC, respectively (see Figure 1C, oligonucleotides D5 and D6). These molecules still adopt the ps conformation (8). In this study we summarize the characteristic features of the ps molecules we have examined to date.

### *Materials and Methods*

*Oligonucleotide Synthesis and Characterization.* Oligonucleotides ps-C8, ps-C10, ps-G10, aps-C8, aps-C10, and aps-G10 (Figure 1A) were synthesized by modifications of standard phosphoramidite chemistry and purified as described elsewhere (2). The oligonucleotides constituting the linear duplexes were prepared according to Refs. 3 and 5. All solutions contained a standard buffer, 10 mM Na-cacodylate, pH 7.2, in addition to the specified salts (NaCl, $MgCl_2$). The molar extinction coefficients of the oligonucleotides (Table I) were determined by spectral and phosphate analysis (2,3,5). The DNA duplexes were prepared for measurements by mixing the appropriate oligonucleotides in the desired salt solutions, heating to 50-60°C for 5 minutes, and cooling slowly to room temperature. DNA concentrations are given in nucleotide + terminal nucleoside units.

An amino group was introduced at the the 5′ end of the F-series oligonucleotides (Figure 1D) by an extra cycle of phosphoramidite synthesis with Aminolink-1 (4-dimethylamino-pyridine, Applied Biosystems). The presence of the 5′-amino group in fractions obtained during oligonucleotide purification was demonstrated by a spot test with fluorescamine (Sigma).

*Spectroscopy.* Ultraviolet absorption measurements were made with a Uvikon 820 spectrophotometer equipped with computer-controlled thermostated cuvette holders and data acquisition. Spectra were recorded in steps of 2 nm from 220 to 320 nm in 4° intervals for both heating and cooling cycles in the range from 2 to 96°C. The data sets were corrected, analyzed and plotted as described elsewhere (6). Circular dichroism (CD) spectra were acquired on a Jobin Yvon Model IV Dichrograph with a resolution of 1 nm. $^{31}$P-NMR spectra were measured with a Bruker AM 360L spec-

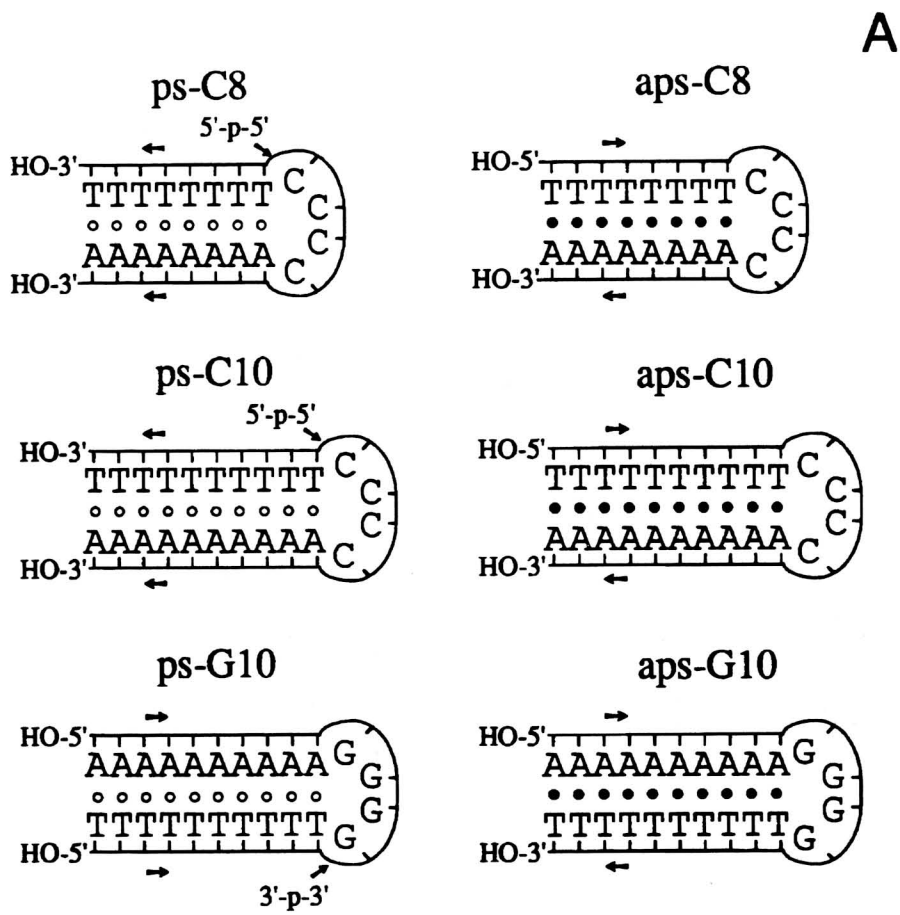


B

```
C2: 5'-ATTAAATTTTAAAAATTTTTT-3'
      oooooooooooooooooooo
    5'-TAATTTAAAATTTTTAAAAAA-3' :C3

C3: 5'-TAATTTAAAATTTTTAAAAAA-3'
      ••••••••••••••••••••
    3'-ATTAAATTTTAAAAATTTTTT-5' :C7
```

**Figure 1:** *Oligonucleotide hairpins and linear duplexes in the ps and aps conformations.* The Watson-Crick conventional *cis*-base pairs of the antiparallel stem regions are shown by the symbol (●) and the *trans*-Watson-Crick base pairs of the parallel stranded duplex by the symbols (○) for the dA · dT and (□) for the dG · dC base pairs. (A) Hairpin structures (2). The unusual phosphodiester bonds (5'-p-5' and 3'-p-3') in the ps hairpins are indicated. (B) C-series duplexes (3).

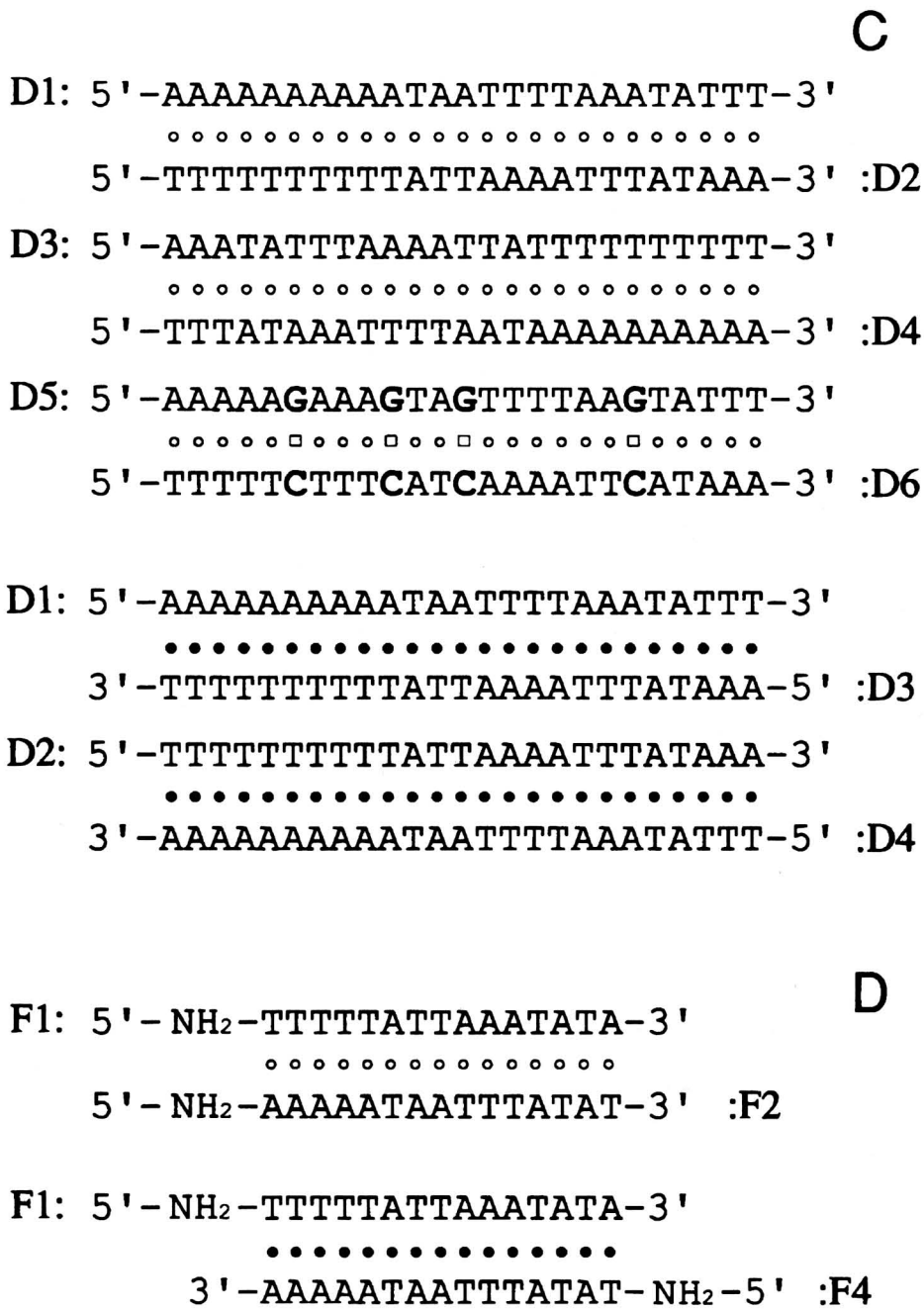


**Figure 1** *continued*

(C) D-series duplexes (5,8). (D) F-series duplexes. Oligonucleotides F1, F2, F3 and F4 were synthesized with an amino group at the 5′ end. In all cases, the formation of base paired structures was established electrophoretically as well as by other means (2,3,5,8, this study).

**Table I**
Ultraviolet Absorption of ps and aps Duplexes[a]

| DNA duplex | Extinction coefficients[b] in 0.1 M NaCl, 20°C | | | Absorbance ratios in 0.1 M NaCl, 20°C | | | $\frac{A_{250}}{A_{284}}$ in 0.1 M NaCl | |
|---|---|---|---|---|---|---|---|---|
| | $\lambda_{max}$ | $\varepsilon_{max}$ | $\varepsilon_{260}$ | $\frac{A_{250}}{A_{260}}$ | $\frac{A_{280}}{A_{260}}$ | $\frac{A_{290}}{A_{260}}$ | 20°C | 80°C |
| *Parallel Stranded Duplexes* | | | | | | | | |
| ps-C8 | 258 | 7.9 | 7.9 | 0.83 | 0.49 | 0.13 | 2.4 | 2.2 |
| ps-C10 | 259 | 7.9 | 7.8 | 0.85 | 0.48 | 0.12 | 2.5 | 2.3 |
| ps-G10 | 257 | 8.7 | 8.4 | 0.92 | 0.43 | 0.13 | 3.0 | 2.6 |
| ps-F1 · F2[c] | 260 | 7.2 | 7.2 | 0.81 | 0.43 | 0.09 | 3.3 | 2.8 |
| ps-C2 · C3 | 258 | 7.0 | 6.9 | 0.85 | 0.42 | 0.09 | 3.1 | 2.7 |
| ps-D1 · D2 | 258 | 7.0 | 7.0 | 0.84 | 0.41 | 0.08 | 3.2 | 2.7 |
| ps-D3 · D4 | 258 | 7.1 | 7.0 | 0.84 | 0.40 | 0.08 | 3.3 | 2.7 |
| ps-D5 · D6[c] | 258 | 6.9 | 6.9 | 0.86 | 0.44 | 0.12 | 2.9 | 2.5 |
| *Antiparallel Stranded Duplexes* | | | | | | | | |
| aps-C8 | 260 | 7.1 | 7.1 | 0.82 | 0.62 | 0.20 | 1.8 | 2.3 |
| aps-C10 | 261 | 6.9 | 6.9 | 0.80 | 0.62 | 0.20 | 1.8 | 2.2 |
| aps-G10 | 258 | 7.6 | 7.6 | 0.89 | 0.56 | 0.19 | 2.1 | 2.6 |
| aps-F1 · F4[c] | 260 | 6.8 | 6.8 | 0.77 | 0.51 | 0.14 | 2.2 | 2.7 |
| aps-C3 · C7 | 260 | 6.1 | 6.1 | 0.79 | 0.55 | 0.16 | 2.0 | 2.7 |
| aps-D1 · D3 | 260 | 6.0 | 6.0 | 0.77 | 0.56 | 0.16 | 2.0 | 2.8 |
| aps-D2 · D4 | 260 | 6.1 | 6.1 | 0.78 | 0.54 | 0.16 | 2.0 | 2.7 |

[a]The subscripts refer to wavelengths in nm. All values were measured in 10 mM Na-cacodylate, pH 7.2. The $Na^+$ concentration including the buffer contribution was 0.11 M. Data in part from Ref. 6.
[b]$\lambda_{max}$ is the wavelength in nm with the highest extinction coefficient; $\varepsilon_{max}$ and $\varepsilon_{260}$ are in units of $mM^{-1}cm^{-1}$.

trometer at the Max Planck Institute for Experimental Medicine, Göttingen, FRG, operating at 145.785 Hz with $^1H$ broad-band decoupling. Chemical shifts refer to 80% phosphoric acid as an external standard.

*Enzymatic Reactions.* The oligonucleotides were end-labeled with [$^{32}P$] to a specific activity of $10^5$ cpm $nmol^{-1}$ with T4 polynucleotide kinase (New England Biolabs). Nuclease studies were carried out in the following buffers: (i) DNase I (Cooper Biomedicals): 40 mM Tris-HCl, pH 7.5, 3.3 mM $MgCl_2$, 0.2 mM $CaCl_2$. (ii) *Escherichia coli* exonuclease III (New England Biolabs): 50 mM Tris-HCl, pH 8.0, 5 mM $MgCl_2$, 10 mM 2-mercaptoethanol. The products of the enzymatic degradation were examined by polyacrylamide gel electrophoresis under denaturing conditions: 20% polyacrylamide (5% crosslinking), 8 M urea, 90 mM Tris-borate, 2 mM Na-EDTA, pH 8.0, 70°C.

*Drug Binding and Energy Transfer.* Fluorescence measurements were made with an SLM 8000 photon counting spectrofluorimeter. DNA additions were made with a 25 µl Hamilton microsyringe dispenser unit maintained at a temperature not higher

than that of the thermostated cuvette. The emission spectra were corrected by internal standards and smoothed with Chebyshev polynomials after background subtraction.

*Preparation of Fluorescently Labeled Amino-Oligonucleotides.* Fluorescein-5'-isothiocyanate (FITC, Molecular Probes) was dissolved in dimethylformamide to a concentration of 10 mg/ml. Twenty µl of the reagent were added to 1.0 optical density unit (ODU) of oligonucleotides F1 or F3 in a total volume of 100 µl of 0.3 M Na-carbonate buffer, pH 9.5, and incubated 4 hours in the dark at room temperature. The reaction was quenched by addition of glycine to a final concentration of 10 mM. Labelling of oligonucleotides F2 and F4 with tetramethylrhodamine-5'-isothiocyonate (TRITC; Molecular Probes) was carried out by the same procedure, but in 0.2 M carbonate buffer pH 9.5 and with addition of 3 µl of an 80 mg/ml solution of the reagent in methylsulfoxide. The reacted oligonucleotides were purified by (i) spin-column gel filtration with Sephadex G25-Superfine (Pharmacia), and (ii) reverse phase FPLC (Pharmacia).

*Model Force Field Calculations.* To construct the different ps and aps structures a modified version of the AMBER package (Refs. 2 and 3 and citations therein) was used in conjunction with the INSIGHT (Biosym Tech.) molecular modelling package and a PS390 Evans and Sutherland graphics workstation.

## *Results and Discussion*

### *Spectroscopic Properties*

An overview of the spectroscopic properties of ps-D1 · D2 compared to aps-D1 · D3 is given in Figure 2. The results are representative for the other ps molecules examined to date (Table I) with the exception of the $^{31}$P-NMR spectra which have only been recorded with the indicated duplexes. The UV spectra of the native ps molecules show a blue shift relative to the aps references, whereas the spectra in the denatured state are nearly identical. The distinctive absorption spectrum of native ps-DNA presumably reflects particular features of the electronic structure and stacking geometry. A plot of the ratio of the absorbances in the denatured and native states versus wavelength emphasizes the characteristic differences between ps-DNA and aps-DNA in a manner independent of concentration (Figure 2B1,B2). By judicious choice of wavelengths, absorbance ratios can be derived which emphasize the qualitative differences in the spectra and melting temperature of ps- and aps-DNAs (Figure 2B3, Table I). Thus the $A_{250}/A_{284}$ ratio decreases in the case of ps-DNA but increases upon denaturation of aps-DNA. The CD spectra confirm the existence of a native duplex structure with both the ps and aps pairs of oligonucleotides but the differences in circular dichroism between 260 and 290 nm indicate that the conformations are not the same (Figure 2C).

$^{31}$P-NMR spectra of ps-D1 · D2 and aps-D1 · D3 have been measured in the native and denatured states (K. Rippe, N.B. Ramsing, F. Eckstein, T.M. Jovin, in preparation). It is evident from Figures 2D1,D2 that the backbone structures of ps-D1 · D2 and aps-D1 · D3 are dissimilar. The distinctions (broader, downfield shifted spectrum

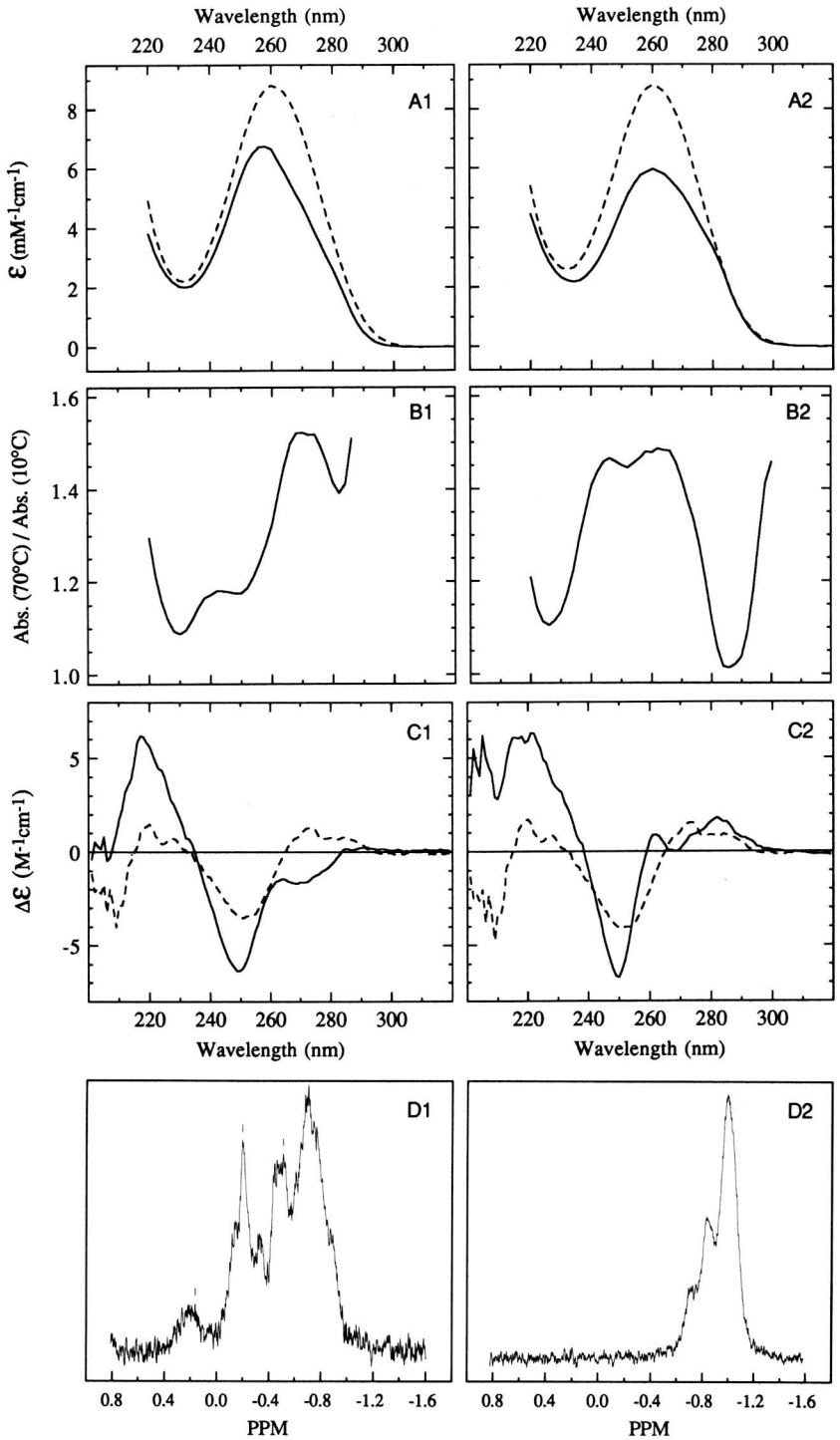
Wavelength (nm)
220 240 260 280 300
A1
A2
ε (mM-1cm-1)
8
6
4
2
0
B1
B2
Abs. (70°C) / Abs. (10°C)
1.6
1.4
1.2
1.0
C1
C2
Δε (M-1cm-1)
5
0
-5
D1
D2
0.8 0.4 0.0 -0.4 -0.8 -1.2 -1.6
PPM

Figure 2

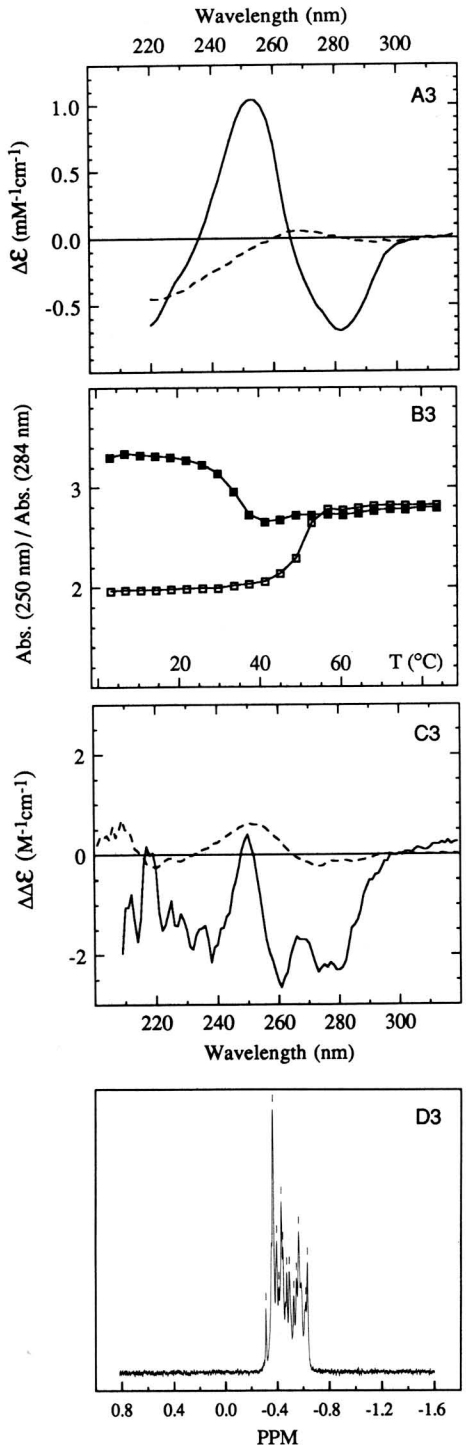


**Figure 2:** *Spectroscopic properties of ps-D1 · D2 and aps-D1 · D3 duplexes.* (A1, B1, C1, D1) ps-D1 · D2. (A2, B2, C2, D2) aps-D1 · D3. (A1, A2) UV-spectra at 10°C (—) and at 70°C (----). (A3) UV difference spectra (ps − aps) at 10°C (—) and at 70°C (----). (B1, B2) Hyperchromicity spectra expressed as the ratio of absorbances at 70°C and 10°C. (B3) Wavelength dependent melting curve of ps-D1 · D2 (■) and aps-D1 · D3 (□). The ratio of UV absorbances at 250 nm and 284 nm is plotted versus temperature. (C1, C2) CD spectra at 10°C (—) and at 70°C (----). Δε is the difference in the molar extinction coefficients for right and left polarized light. (C3) CD difference spectra (ps − aps) at 10°C (—) and at 70°C (----). ΔΔε is the difference between the Δε values for the ps and aps structures. (D1, D2) $^{31}$P-NMR spectra at 20°C. (D3) $^{31}$P-NMR spectra of ps-D1 · D2 at 55°C. All spectra in 2 mM $MgCl_2$ and 10 mM Na-cacodylate, pH 7.2, except for the $^{31}$P-NMR (see D) data that were recorded in 50 mM NaCl, 25 mM Na-cacodylate, pH 6.8, 25 mM EDTA, and 50% $D_2O$.

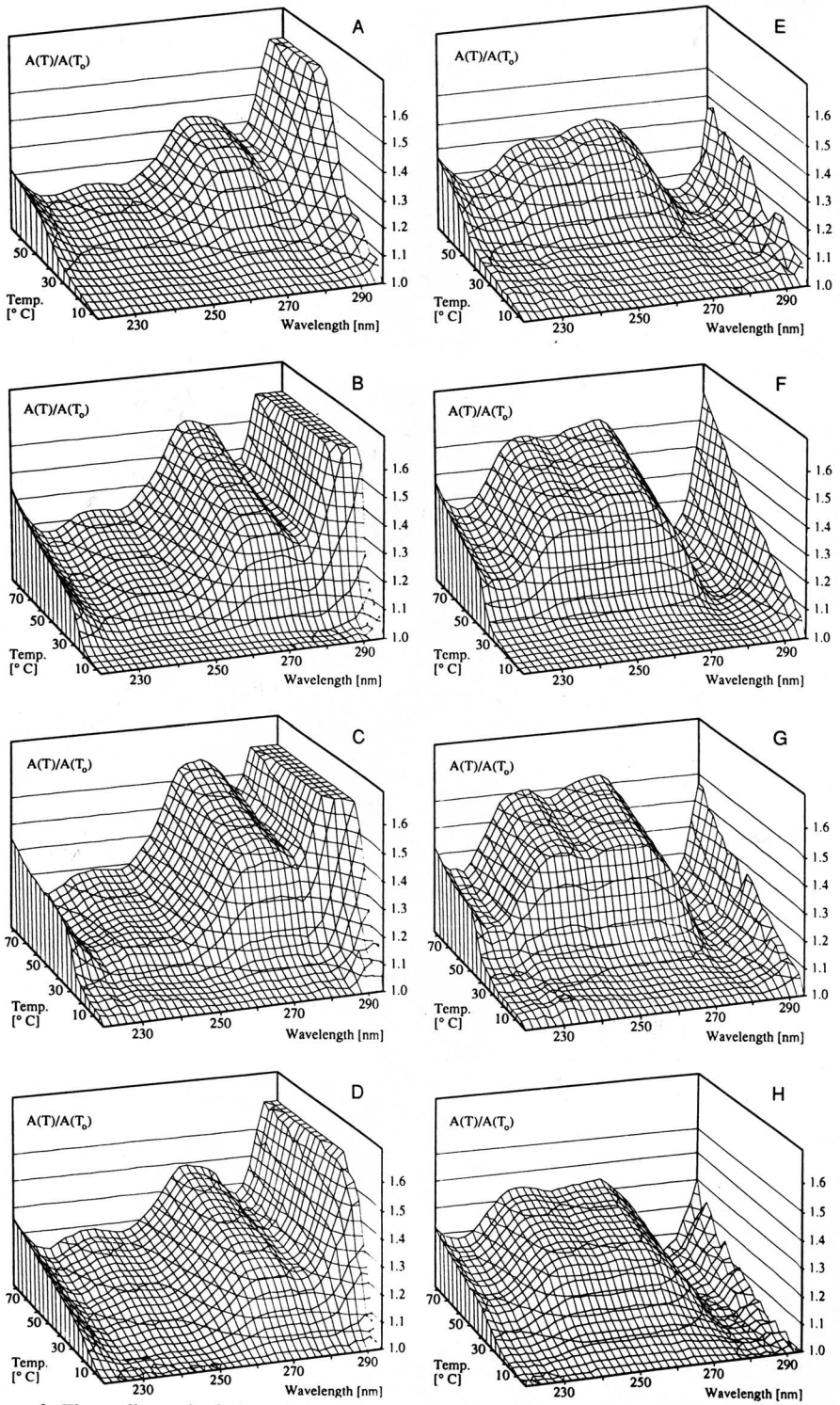


**Figure 3:** *Thermally-resolved ultraviolet absorption spectra of ps and aps helices.* The ratio of $A_\lambda(T)/A_\lambda(T_o)$, where $T_o$ is the initial temperature is plotted versus temperature. Left column: parallel stranded DNAs: (A) ps-C10; (B) ps-C2 · C3; (C) ps-D3 · D4; (D) ps-F1 · F2. Right column: antiparallel stranded DNAs: (E) aps-C10; (F) aps-C3 · C7; (G) aps-D2 · D4; (H) aps-F1 · F4. All spectra in 0.1 M NaCl, 10 mM Na-cacodylate, pH 7.1, except for (D) and (H) that were measured in 0.4 M NaCl.

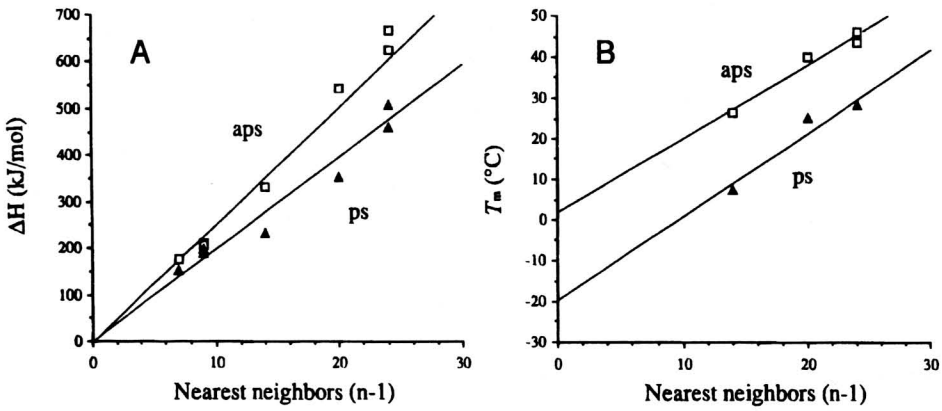


**Figure 4:** *Length dependence of the van'Hoff enthalpy of melting $\Delta H_{vH}$ and melting temperature $T_m$.* The ps duplexes are shown by the symbol (Δ) and the aps duplexes by (□). (A) Dependence of $\Delta H_{vH}$ upon number of nearest neighbor interactions N.N. = $(n-1)$, where $n$ is the length of the base paired region. The slope of the regression line the mean value of $\Delta H_{vH}$ per nearest neighbor ($\Delta H_{vH}$/N.N.), which for the ps molecules is $\Delta h$ = 19.9 kJ mol$^{-1}$ and for aps molecules $\Delta h$ = 25.3 kJ mol$^{-1}$. (B) Dependence of $T_m$ on $(n-1)$. The hairpins are not shown because their $T_m$ is independent of concentration and is higher. The $T_m$ values of the linear duplexes were scaled to a concentration of 2 μM strands. The solid lines are linear regressions with slopes of 1.8°C/N.N. for the aps and 2.1°C/N.N. for the ps duplexes.

**Table II**
Thermodynamic Data for Helix-Coil Transitions of ps-DNA and aps DNA[a]

| DNA duplex | $\Delta H_{vH}$[b] (kJ/mol) | | $T\Delta S$[c] (kJ/mol, 25°C) | | $\Delta G$[d] (kJ/mol, 25°C) | |
|---|---|---|---|---|---|---|
| | NaCl (0.1-1.0 M) | $MgCl_2$ (0.5-8 mM) | NaCl (0.1 M) | $MgCl_2$ (2 mM) | NaCl (0.1 M) | $MgCl_2$ (2 mM) |
| ps-C8 | 152 8 | 160 6 | 147 8 | 152 7 | 5 8 | 8 8 |
| ps-C10 | 198 2 | - | 188 2 | - | 10 2 | - |
| ps-G10 | 190 8 | - | 180 8 | - | 10 8 | - |
| ps-F1 · F2 | 231* | - | 210* | - | 22* | - |
| ps-C2 · C3 | 353 13 | 400 15 | 317 15 | 353 15 | 36 2 | 47 8 |
| ps-D1 · D2 | 459 3 | 507 2 | 418 3 | 453 2 | 41 <1 | 54 <1 |
| ps-D3 · D4 | 507 2 | 542 2 | 466 2 | 484 2 | 42 <1 | 58 <1 |
| ps-D5 · D6 | 372 2 | 451 1 | 414 2 | 349 1 | 23 <1 | 37 <1 |
| aps-C8 | 177 6 | 192 4 | 166 6 | 177 4 | 11 6 | 15 4 |
| aps-C10 | 212 3 | - | 195 3 | - | 17 3 | - |
| aps-G10 | 206 6 | - | 189 6 | - | 16 6 | - |
| aps-F1 · F4 | 334* | - | 296* | - | 38* | - |
| aps-C3 · C7 | 546 6 | 610* | 484 6 | 532* | 62 3 | 78* |
| aps-D1 · D3 | 670 4 | 736 3 | 590 4 | 641 4 | 80 2 | 95 2 |
| aps-D2 · D4 | 628 2 | 669 2 | 555 2 | 581 2 | 73 1 | 88 1 |

[a]The listed parameters are average values obtained from numerous experiments with 0.1-1.0 M NaCl or 0.5-8 mM $MgCl_2$, and 10 mM Na-cacodylate, pH 7.2. Analysis of both the increasing and decreasing temperature slopes are included. The small number beside each entry is the relative magnitude of the 95% confidence limits in %. For example, 152 8, signifies an average value of 152 with a 95% confidence limit of 8%, that is, ±12. Data in part from Refs. 6 and 8.

[b]$\Delta H_{vH}$ is the average van't Hoff enthalpy of melting. No correlation with salt concentration in the range 0.1-1.0 M NaCl or 0.5-8 mM $MgCl_2$ is observed.

[c]$T\Delta S$ is the product of the temperature, $T$(298.1 K) and entropy of melting, $\Delta S$, at 25°C in 0.1 M NaCl (the $Na^+$ concentration including the buffer contribution was 0.11 M). The entropy was calculated by using the average $\Delta H_{vH}$ and the $T_m$ in 0.1 M NaCl and 2 mM $MgCl_2$ calculated from linear regressions (Table III).

[d]$\Delta G$ is the average Gibbs free energy of transition, calculated by using the average $\Delta H_{vH}$ and the estimate of $T\Delta S$.

*Indicates that too few measurements were made to calculate 95% confidence limits.

of ps-DNA) disappear upon thermal denaturation (Figure 2D3), as in the case of the other spectroscopic techniques. Such data yield information about the structure of the sugar-phosphate backbone, inasmuch as the chemical shifts are influenced primarily by the P-O torsion angles and O-P-O bond angles (9). Although we are not able as yet to assign peaks to particular phosphate residues in the sequences, we interpret the broadening of the spectrum of the native ps duplex as indicative of greater flexibility of the sugar-phosphate constituents of the backbone (Figure 2D1).

### *Helical Stability*

The systematic comparison of the ps-DNA constructs with the reference aps duplexes is particularly advantageous in studies of relative thermodynamic stability. For

**Table III**
Salt Dependence of Melting Temperatures[a]

| | $T_m$[b] | | $\frac{1}{T_m} = \alpha + \beta \cdot \log_{10}(c)$[c] | | | | $\frac{\partial T_m}{\partial \log_{10}(C)}$[d] | |
|---|---|---|---|---|---|---|---|---|
| | NaCl | $MgCl_2$ | NaCl (M) | | $MgCl_2$ (mM) | | NaCl | $MgCl_2$ |
| DNA duplex | (°C, 0.1 M) | (°C, 2 mM) | $\alpha \cdot 10^3$ ($K^{-1} \cdot 10^3$) | $\beta \cdot 10^3$ ($K^{-1} \cdot 10^3$) | $\alpha \cdot 10^3$ ($K^{-1} \cdot 10^3$) | $\beta \cdot 10^3$ ($K^{-1} \cdot 10^3$) | (°C) | (°C) |
| *Parallel stranded duplex* | | | | | | | | |
| ps-C8 | 33.5 2 | 41.0* | 3.10 <1 | −0.17 8 | - | - | 16 9 | - |
| ps-C10 | 39.4 1 | - | 3.01 <1 | −0.19 7 | - | - | 19 8 | - |
| ps-G10 | 40.6 1 | - | 3.01 <1 | −0.18 5 | - | - | 18 6 | - |
| ps-F1 · F2 | 7.5* | - | - | - | - | - | - | - |
| ps-C2 · C3 | 25.1 4 | 33.8* | 3.19 <1 | −0.17 13 | - | - | 15 12 | - |
| ps-D1 · D2 | 28.5 4 | 35.7* | 3.11 <1 | −0.21 12 | - | - | 17 10 | 7† |
| ps-D3 · D4 | 28.4 5 | 37.4 2 | 3.11 <1 | −0.22 17 | 3.26 <1 | −0.10 12 | 19 14 | 10 11 |
| ps-D5 · D6 | 15.1 1 | 25.6 1 | 3.26 <1 | −0.21 4 | 3.38 <1 | −0.11 6 | 18 5 | 10 5 |
| *Antiparallel stranded duplexes* | | | | | | | | |
| aps-C8 | 44.7 2 | 49.7* | 3.00 <1 | −0.15 17 | - | - | 15 8 | - |
| aps-C10 | 50.4 1 | - | 2.93 <1 | −0.16 11 | - | - | 17 11 | - |
| aps-G10 | 50.5 2 | - | 2.93 <1 | −0.16 19 | - | - | 17 17 | - |
| aps-F1 · F2 | 26.5* | - | - | - | - | - | - | - |
| aps-C3 · C7 | 40.0 2 | 46.8* | 3.04 <1 | −0.16 11 | - | - | 16 9 | - |
| aps-D1 · D3 | 46.0 2 | 50.8* | 2.97 <1 | −0.17 10 | - | - | 16 8 | 5† |
| aps-D2 · D4 | 43.5 1 | 50.3 2 | 2.99 <1 | −0.17 7 | 3.12 <1 | −0.09 11 | 17 6 | 8 9 |

[a]The listed parameters are obtained from a linear regression of $1/T_m$ and $T_m$ versus $\log(c)$, where $c$ is the concentration of NaCl (0.05-0.5 M) or $MgCl_2$ (0.12-2 mM), with 10 mM Na-cacodylate, pH 7.2, throughout. The experimental $T_m$ values from measurements with linear duplexes were adjusted to a total strand concentration of 2 μM (6). Only results derived from data for increasing temperatures were included in the regressions. The small number beside each entry is the relative magnitude of the 95% confidence limits in %. For example, 33.5 2 signifies an average of 33.5 with a 95% confidence limits of 2%, that is, ±0.7. Data in part from Ref. 6.

[b]$T_m$ is the melting temperature in 0.1 M NaCl (the $Na^+$ concentration including the buffer contribution was 0.11 M) and 2 mM $MgCl_2$ with a total strand concentration of 2 μM. It was calculated from the linear regression of $1/T_m$ versus $\log_{10}(c)$.

[c]Linear regression coefficients for $1/T_m$ as a function of $\log_{10}(c)$. α is the intercept and β the slope of the regression line.

[d]The slope of linear regression of $T_m$ versus $\log_{10}(c)$.

*Indicates that too few measurements were made to calculate the 95% confidence limits.

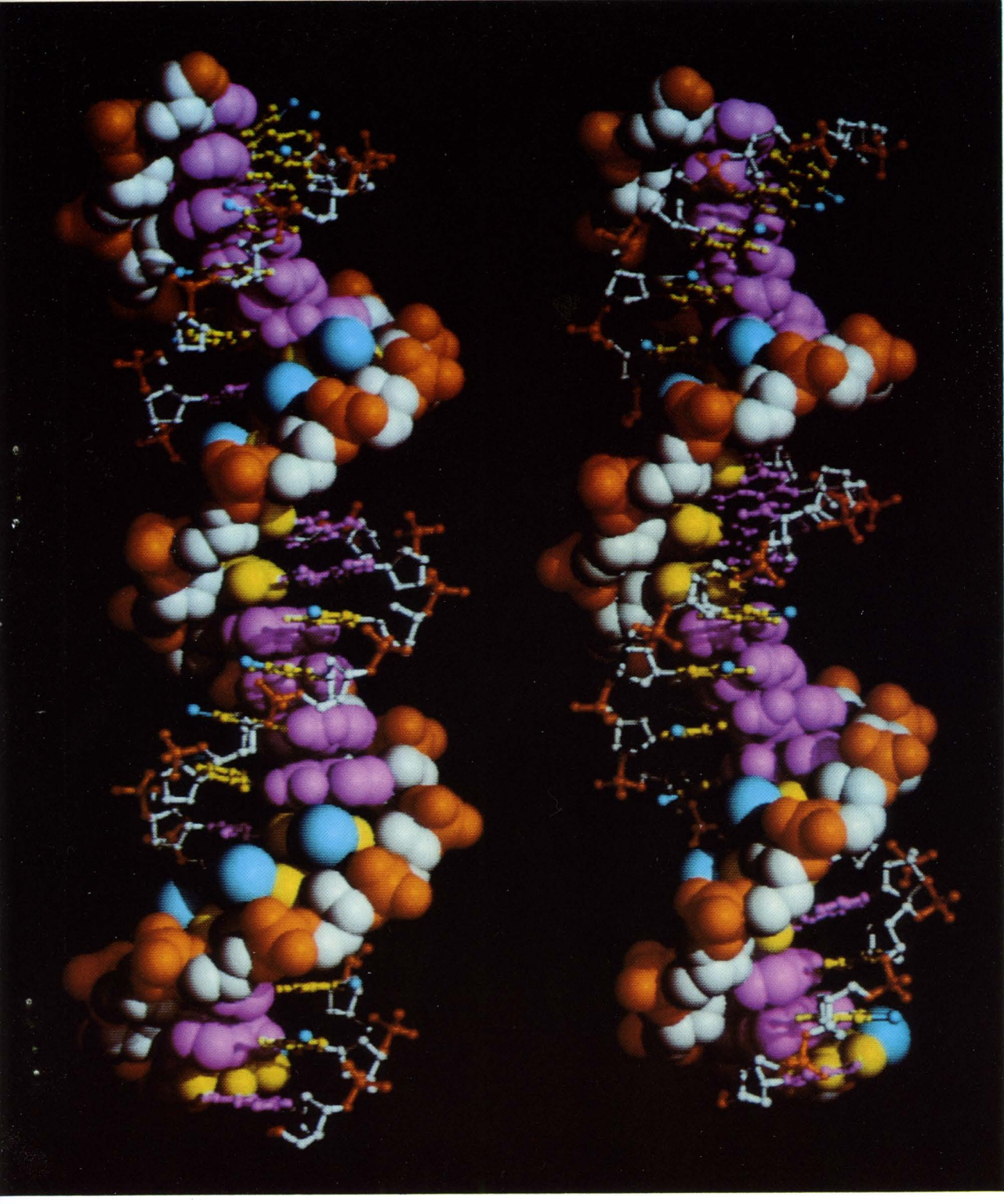

**Figure 9:** *3-D models of the optimized double-stranded 21-nt ps-C2 · C3 (left) and aps-C3 · C7 (right).* In both cases, the common strand (C3) is shown as a space filling structure and the other strands in a ball-stick representation. Such a split display, generated with the SCHAKAL v86b program of Dr. E. Keller, Univ. of Freiburg, F.R.G., improves the perception of details within models of helical nucleic acids. Color coding: sugars, white; phosphates (including O3′ and O5′) red; adenine, cyan; thymine, yellow; thymine methyl groups, megenta. In other axial orientations, a distinct curvature is perceived in both structures, the potential significance of which is under investigation using a version of the AMBER program incorporating a formalism for ion-ion and ion-DNA interactions (26).

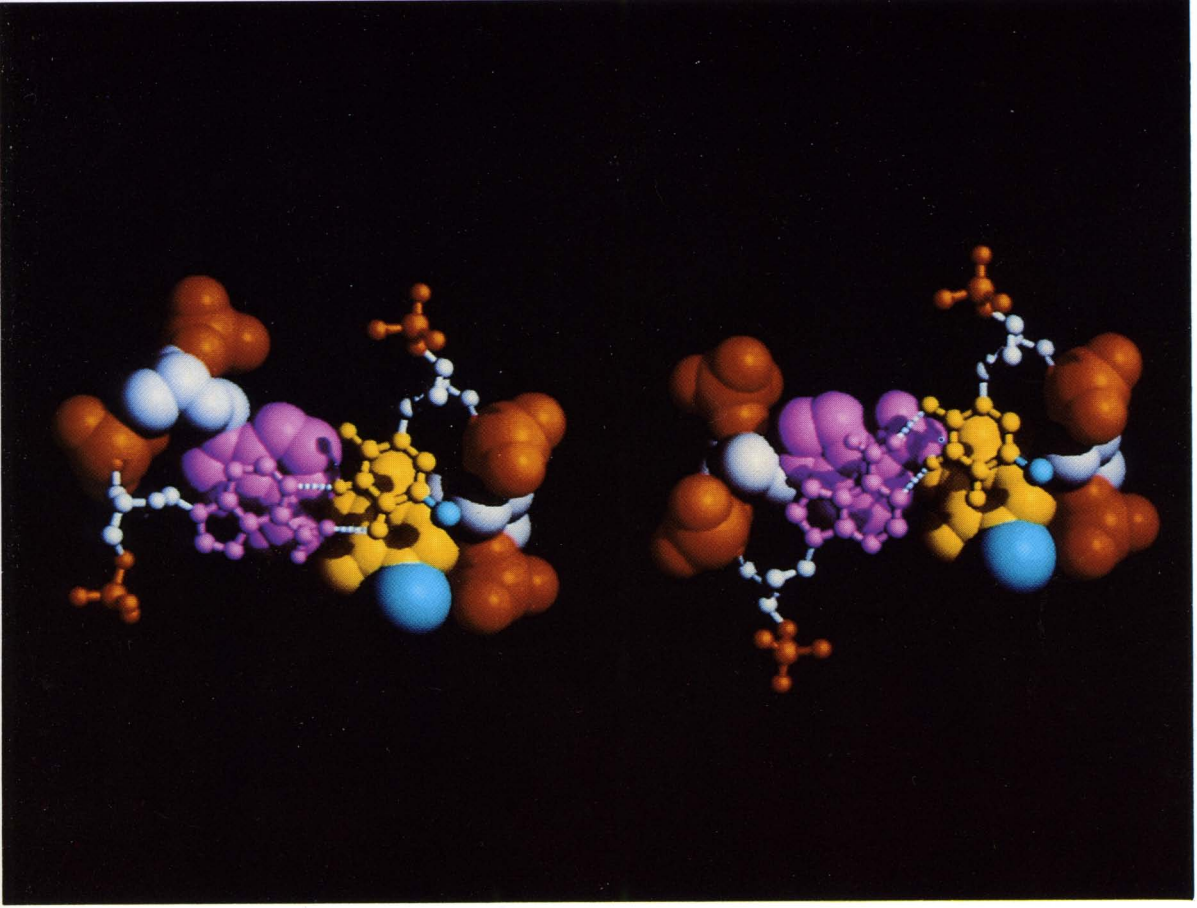

**Figure 10:** *Models of dA-dT base pairs in optimized aps (left) and ps (right) DNA structures.* Color coding as in Figure 9. A dinucleotide section is shown with the upper base pair (towards the viewer) as a ball-stick model; probable hydrogen bonds appear as broken white lines. The *trans* configuration of ps-DNA lacks the distinctions leading to a minor (top) and major groove (bottom) in aps-DNA.

example, in the case of the D-series of molecules (Figure 1C), each oligonucleotide was examined in both the ps and the aps conformation. The thermally induced helix-coil transitions measured by UV absorption spectroscopy are best visualized by normalizing the absorbances at each temperature $T$ and wavelength to the values at the initial (low) temperature $T_o$. The resultant three-dimensional plots (Figure 3) reveal for all members of the ps and aps groups, respectively, the characteristic differences alluded to earlier (3,5,6) The results from the analysis of the thermal transition are summarized in Figure 4 and in Tables II and III.

The important findings are: (i) All species demonstrate reversible thermal transitions in $MgCl_2$ (0.5-8 mM) and NaCl (0.05-1.6 M). (ii) Very good fits to a concerted two state transition model are achieved, the primary parameters of which are the melting temperature $T_m$ and van't Hoff melting enthalpy $\Delta H_{vH}$. (iii) The $T_m$ increases with salt concentration in a classical manner ($\partial T_m/\partial \log_{10}[NaCl] = 17 \pm 2°$), but is lower by $\sim 10°$ and $15°$, respectively, for the hairpins and duplexes in the ps relative to the aps conformation (Table III). (iv) The divalent cation $Mg^{2+}$, even at low concentrations $\leqslant 2$ mM, strongly stabilizes ps-DNA, as reflected in the increased $T_m$ as well as in the magnitude of both $\Delta H_{vH}$ and $\Delta G$ (Table II). (vi) $\Delta H_{vH}$ appears independent of the salt concentration and is $\sim 20\%$ lower in the case of the ps-DNAs. (vi) The data for the various DNA species can be normalized to the number of nearest neighbor interactions (N.N. $\equiv$ chain length $- 1 = n - 1$), thereby revealing a rather consistent picture (Figure 4). Average enthalpy changes per mole of nearest neighbor interaction, $\Delta h$, obtained from the slopes of the lines in Figure 4A, are 20 kJ $mol^{-1}$ for ps-DNA and 25 kJ $mol^{-1}$ for aps-DNA in NaCl; the values in $Mg^{2+}$ are $\sim 7$-$17\%$ higher. The values for individual oligonucleotides show systematic deviations in both $Na^+$ and $Mg^{2+}$, which we attribute to differences in nearest neighbor frequencies and nucleation probabilities. The $T_m$ for aps and ps duplexes varies with chain length by $\sim 1.8°$ and $2.1°$ per residue, respectively (Figure 4B).

### *Drug Binding*

The interactions of the DNA specific dyes bis-benzimidazole H-33258 (BBI-258), 4′, 6-diamidine-2-phenylindol (DAPI), and ethidium bromide are characterized by a significant enhancement of fluorescence upon binding with B-DNA, i.e., the aps constructs (Figure 5). However, in the case of ps-DNA, only the intercalator ethidium binds to a significant degree and with an affinity actually higher than that for aps-DNA (Figure 5C) (2,3). Both BBI-258 and DAPI have been shown to bind within the minor groove of A-T rich regions in B-DNA (10-12). Thus, the reduced fluorescence with the ps molecules probably reflects differences in the pattern of hydrogen bonding sites and other stereochemical features of the grooves of the ps helix compared to the minor groove of B-DNA (Figures 8 and 9).The facilitation of intercalation may be related to the somewhat greater helical rise of the ps duplex estimated from model calculations (see below).

Conformational transitions of macromolecules can be almost invariably coupled to changes in ligand binding, as exemplified in the case of DNA by the highly cooperative B-Z isomerization (13,14). Numerous small molecules with binding

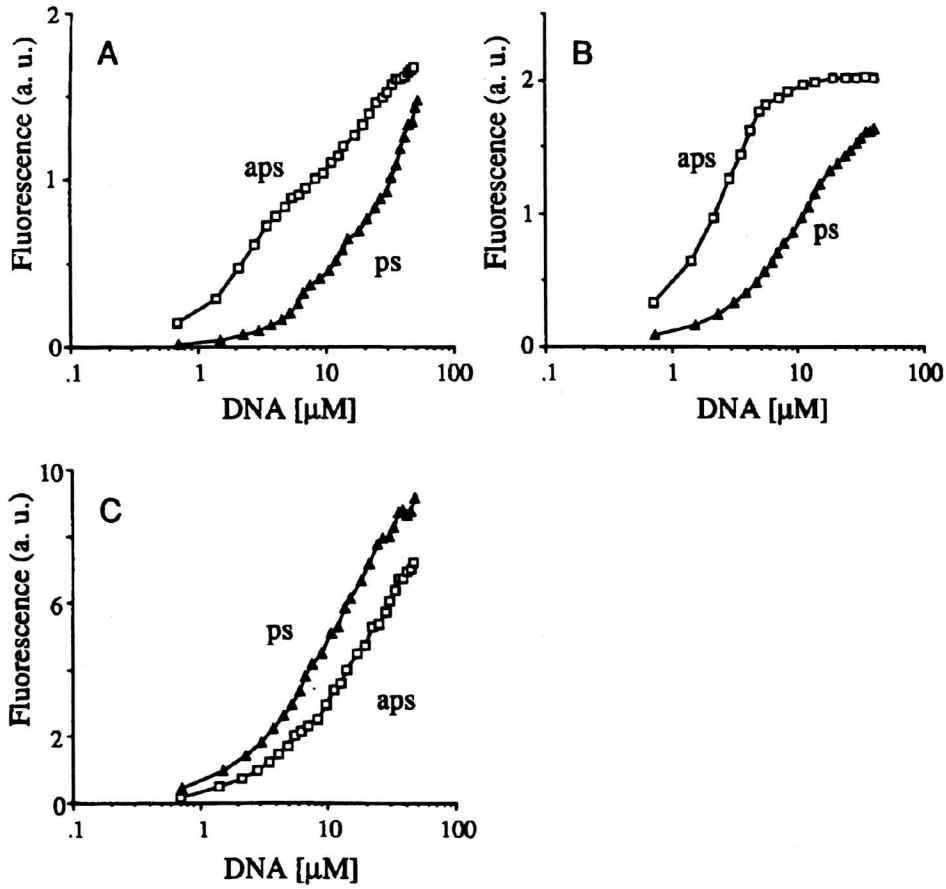


**Figure 5:** *Drug binding to ps-D3 · D4 and aps-D2 · D4 duplexes.* Titration of different fluorescent dyes with ps-D3 · D4 (Δ) and aps-D2 · D4 (□). (A) 0.5 μM BBI-258 in 2 mM $MgCl_2$ at 5°C. $\lambda_{ex}$ = 355 nm, $\lambda_{em}$ = 465 nm. (B) 0.5 μM DAPI in 0.1 M NaCl at 5°C. $\lambda_{ex}$ = 368 nm, $\lambda_{em}$ = 446 nm. (C) 0.5 μM ethidium bromide in 0.1 M NaCl at 5°C. $\lambda_{ex}$ = 520 nm, $\lambda_{em}$ = 610 nm.

specificity for one of the two conformations exist, one of them being ethidium, the addition of which to the high salt left-handed Z form of poly[d(G-C)] induces the reverse transition to the B conformation (15). In view of the apparent facilitation of ethidium intercalation in ps-DNA, it was important to establish whether similar processes are involved. To this end, we synthesized DNA oligonucleotides end-labeled with fluorescent probes suitable for fluorescence resonance energy transfer (FRET) determinations. FRET provides a sensitive "spectroscopic ruler" (16) with a resolution in the range of 10 nm, and has been applied recently to other proximity studies of DNA (17,18). The photophysical basis of the method is the transfer of excitation energy between a donor and an acceptor chosen such that the absorption spectrum of the latter overlaps the emission spectrum of the former. The transfer efficiency depends upon the 6th power of the separation distance as well as on the relative orientations of the donor and acceptor. For the donor-acceptor pair we employed fluorescein (*fl*) and tetratmethylrhodamine (*tmRh*), for which the critical

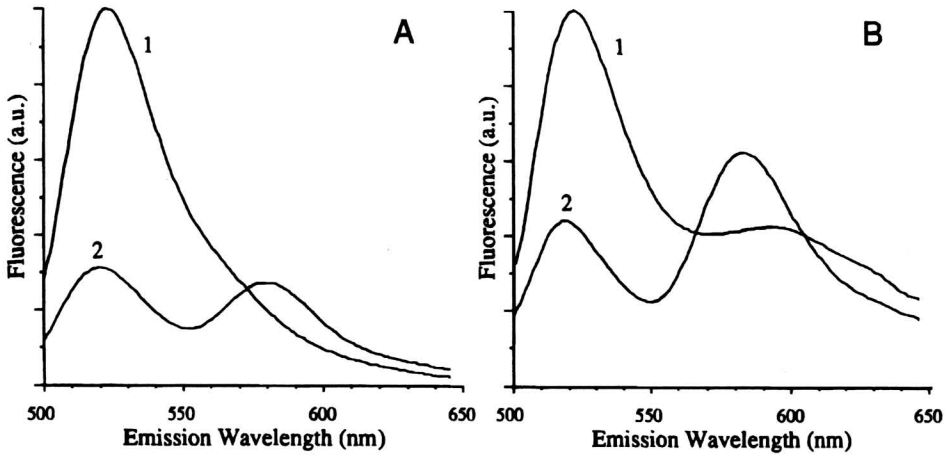


**Figure 6:** *Fluorescence emission spectra of dye labeled ps-F1 · F2 duplexes.* Curve 1 represents the donor emission of a duplex of with fluorescein labeled F1 and unlabeled F2, ps-[*fl*-F1 · F2]. Curve 2 corresponds to a duplex of F1 and F2 labeled at the 5′ end with fluorescein and tetramethylrhodamine, respectively, ps-[*fl*-F1 · *tmRh*-F2]. (A) Emission spectra in 1 mM $MgCl_2$ at 4°C, $A_{260}$ = 0.1, $\lambda_{ex}$ 490 nm. (B) Same conditions as (A) but with the addition of 2 μM ethidium bromide.

distance for 50% transfer ($R_0$) is ~5 nm (19). Fluorescein is also a good donor for the intercalation complex of ethidium. We exploited the potential for dual FRET to demonstrate (i) the formation of a ps duplex with two oligonucleotides labeled at the 5′ termini with donor and acceptor chromophores (FRET *a*); and (ii) intercalation to the ps duplex as evidenced by transfer from the fluorescein donor to intercalated ethidium bromide (FRET *b*). The results of such an experiment are shown by a set of emission spectra in Figure 6. The 15-nt oligonucleotides F1 and F2 (Figure 1D) were labeled with fluorescein and tetramethylrhodamine, respectively. In the case of the ps-[*fl*-F1 · F2] duplex, an unperturbed donor emission is observed with its characteristic peak at ~520 nm (Figure 6A, 1). With the dual labeled ps-[*fl*-F1 · *tmRh*-F2] combination, however, the donor is quenched significantly and the sensitized acceptor (rhodamine) emission appears with a peak at ~580 nm (Figure 6A, 2). A similar effect is observed in the presence of ethidium bromide (Figure 6B) except that both FRET *a* and *b* processes are superposed. That is, transfer from *fl*-F1 to ethidium is evident from the emission shoulder at the dye peak of ~610 nm (Figure 6B, 1). With the dual labeled DNA, the rhodamine acceptor is sensitized at the expense of the alternative ethidium acceptor, the emission of which is consequently diminished (Figure 6B, 2). No FRET is observed at temperatures above the $T_m$ of ps-F1 · F2. Together with other emission and excitation spectra, these results confirm the formation of and intercalation to the ps-F1 · F2 duplex. Further experiments with longer oligonucleotides are in progress in order to establish that the 5′ termini are at the same end of the double helix, the fundamental structural feature of ps-DNA.

*Substrate Specificities.* Ps-DNA shows different substrate properties than B-DNA (Table IV). As an example, the results of digestion with pancreatic DNase I and *E. coli* exonuclease III are shown in Figure 7. Both enzymes exhibit nuclease activity specific for double-stranded structures. DNase I introduces single strand breaks

**Table IV**
Summary of Substrate Properties[a]

| Enzyme activity[b] | ps-DNA | aps-DNA | ss-DNA[c] |
|---|---|---|---|
| Restriction enzymes | | | |
| *Dra*I | − | +++ | ++ |
| *Mse*I | − | +++ | − |
| *Ssp*I | − | + | − |
| DNA nucleases | | | |
| DNase I | − | +++ | +++ |
| Exonuclease III[d] | − | ++ | +++ |
| Bal 31 nuclease | +[e] | +[e] | ++ |
| *S* 1 nuclease | ++ | + | +++ |
| *Micrococcal* nuclease | ++ | + | +++ |
| λ-exonuclease | + | ++ | +++ |
| DNA pol. I, large fragment[f] | +++ | ++ | +++ |
| DNA polymerase I | | | |
| 3′→5′ activity | +++ | ++ | +++ |
| 5′→3′ activity | − | + | + |
| Chemical reagents | | | |
| Phenanthroline-Copper | +[e] | +[e] | + |
| Iron (II)-EDTA | + | + | + |
| Other DNA processing enzymes | | | |
| T4 DNA ligase, blunt end ligation | − | +++ | +++ |
| T4 DNA kinase[g] | +++ | +++ | +++ |

[a]Data from Ref. 7.
[b]Relative enzyme activities: +++, very high; ++, high; +, moderate; −, none or very low.
[c]The ss-DNA apparently also formed aps secondary structures such as aps homoduplexes with mismatches.
[d]Similar results were found also with the ps and aps hairpins (2).
[e]Bal 31 and the phenanthroline-copper complex degrade ps-DNA and aps-DNA at approximately the same rate but show preferred cutting sites only with aps-DNA.
[f]No polymerase activity with ps-DNA (4).
[g]Determined with the ps and aps hairpins (2).

into the B-DNA helix (20) with $Mg^{2+}$ and $Ca^{2+}$ as cofactors whereas exonuclease III from *E. coli* degrades the substrate processively by removing nucleotides from both 3′ ends (21).

DNase I and exonuclease III show a very low level of activity with ps-D1* · D2* compared to aps-D1* · D3* and aps-D2*-D4* (Figure 7A lanes 2-5, Figure 7C lanes 2-7). The experiment with DNase I was also performed at 37°C (Figure 7B). At this temperature, the ps duplex should be melted and, as expected, the activity of DNase I with both the ps and the aps substrates is similar. It follows that the difference in cleavage rate observed at 23°C (Figure 7A) reflects the fundamental distinctions in the helical conformations. The observed susceptibility of the single-stranded substrate to both nucleases (Figure 7A, lanes 6 and 7; Figure 7C, lanes 8-10) may be due to a transient aps secondary structure. It has been shown by X-ray studies of the crystallized complex between DNase I and B-DNA that an exposed loop of the enzyme binds in the minor groove of the DNA (22), a finding consistent with the fact that confor-

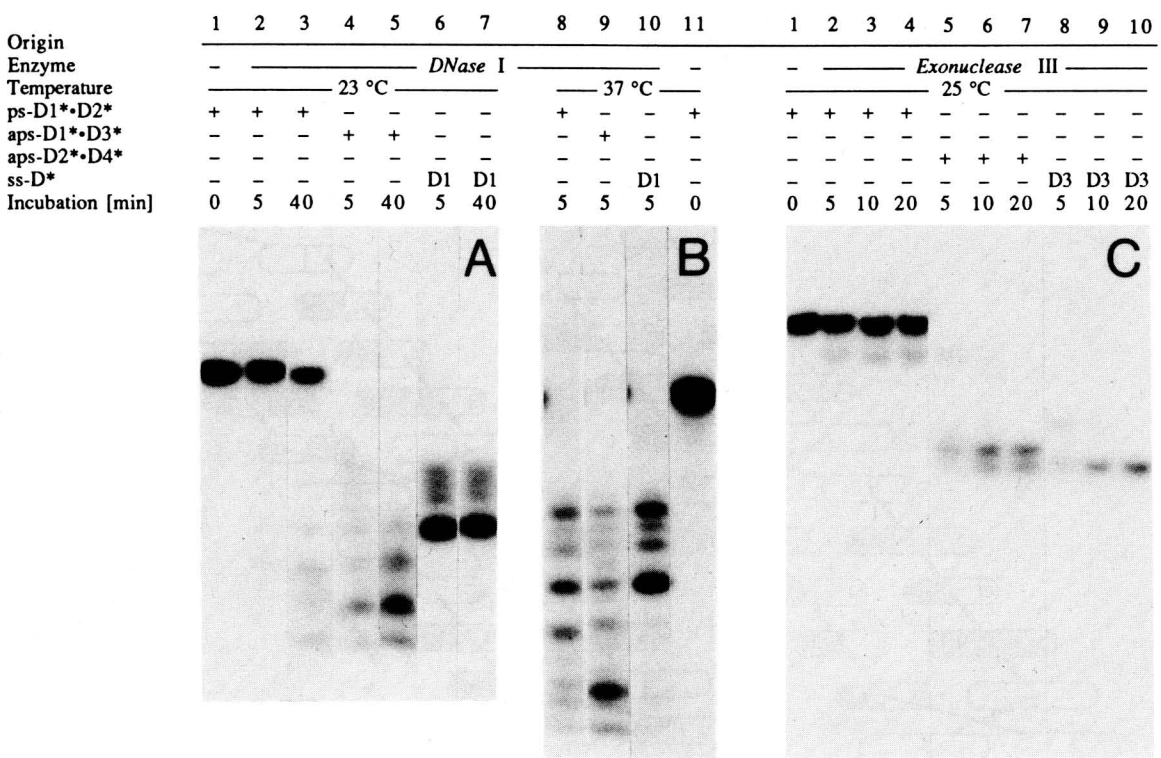


**Figure 7:** *DNase I and exonuclease III digest of ps-D3 · D4 and aps-D1 · D2.* Data from Ref. 7. (A) DNase I: Incubation of 8 U DNase I/nmol nucleotide and 10 μM DNA in 90 μl restriction buffer at 23°C for given time intervals. 14 μl of each sample were run on a denaturing gel. (B) DNase I: Incubation of 8 U DNase I/nmole nucleotide and 10 μM DNA in 90 μl restriction buffer at 37°C for 5 minutes. 14 μl of each sample were run on a denaturing gel. (C) Exonuclease III: 1.3 U/nmole nucleotide, 10 μM DNA in 100 μl restriction buffer at 25°C for given time intervals. 10 μl of each sample were run on a denaturing gel.

mational changes of the minor groove lower the cleavage rate (23). Thus, the reduced activity of DNase I with ps-DNA could be due to the different groove geometry and disposition of functional groups in the ps helix (Figure 8).

### *Influence of dG-dC Base Pairs*

In order to determine if dG and dC residues could be incorporated into the parallel stranded helix, we synthesized two 25-nt variants of the D-series oligonucleotides designated as D5 and D6, in which 4 dA (D5) or 4 dT (D6) bases were replaced by dG and dC, respectively (Figure 1C). A ps-D5 · D6 duplex forms with characteristic UV absorption and CD contributions that can be ascribed to the dG · dC *trans*-base pair (8). The van't Hoff enthalpy difference $\Delta H_{vH}$ for the helix-coil transition of ps-D5 · D6 is reduced by 20% (in NaCl) and 10% (in $MgCl_2$) compared to that of ps-D1 · D2. We calculated that each dG · dC/dA · dT step makes a positive enthalpic contribution to the helical stability of ps DNA that is about half (0.42 in NaCl, 0.66 in $MgCl_2$) that of the dA · dT/dA · dT step.

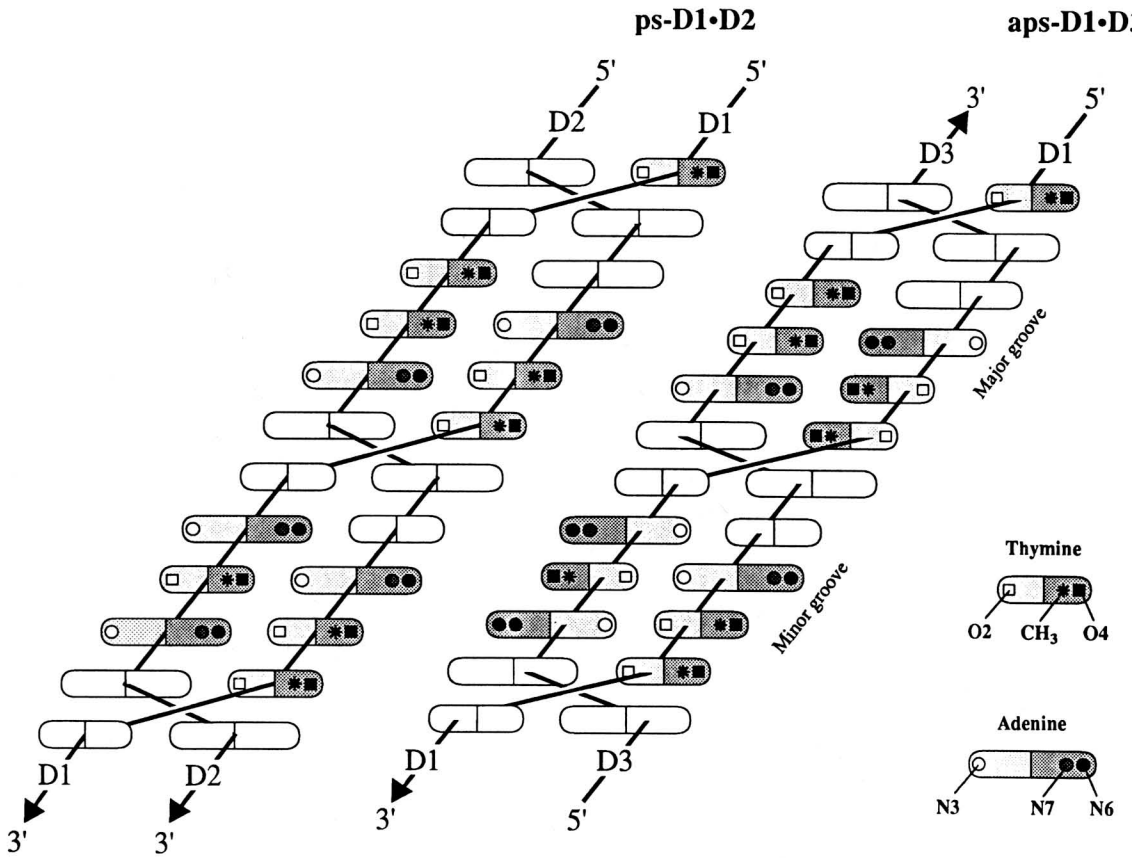


**Figure 8:** *Schematic view of the last 12 bp at the 3' end of ps-D1 · D2 and aps-D1 · D3 laid out in a cylindrical projection.* The sugar-phosphate backbone is shown as a continouous line with the given polarity. The empty base symbols indicate that the nucleotides in those positions are oriented more or less perpendicular to the image plane. Note that the two grooves of ps-DNA cannot be distinguished a priori. That is, the functional groups of both bases project equally into both grooves. The ps helix is also slightly more extended according to model calculations. Adapted from Ref. 7.

*Base Pairing and Model Structure.* The model ps-C2 · C3 and aps-C3 · C7 duplexes in Figure 9 were constructed from the stems of the hairpin structures as described in Refs. 2,3. The characteristic features of ps-DNA perceived in Figure 9 are: (i) parallel polarity of the two strands, (ii) equivalence of the grooves, and (iii) *trans*-Crick-Watson (*reverse* Watson-Crick) base-pairing. The helical twist is comparable to that of the aps helix, but the helical rise is approximately 3% greater. Models for ps-DNA incorporating dG · dC base pairs are presented elsewhere (8).

## *Concluding Remarks*

Next to B-DNA, ps-DNA is the most stable double helical DNA conformation described to date and can exist readily under physiological conditions, given an appropriate sequence complementarity. We note, however, a fundamental distinction between

the equilibria characteristic of isomerization reactions, such as in the B-Z transition (13,14) and those which would involve ps-DNA. One would presume that the latter structure would arise most readily in the course of recombination or exchange reactions; i.e., involving interactions between *separated* segments of DNA (or RNA). For example, the model duplexes discussed in this report (Figure 1C) can formally exchange according to the reaction

$$\text{aps-D1} \cdot \text{D3} + \text{aps-D2} \cdot \text{D4} \leftrightarrow \text{ps-D1} \cdot \text{D2} + \text{ps-D3} \cdot \text{D4}.$$

As discussed in the section on drug binding, environmental conditions (salt, temperature) and the presence of selective ligands would determine the distribution of species. The demonstration that dG · dC base pairs are also compatible with the ps helix (8) extends the potential for this alternative conformation in the case of natural sequences. We have identified elsewhere (3) four canonical situations in which the sequence relationships would comply with the requirements for ps-DNA, the simplest of which involves circularization of single stranded DNA or RNA. Although experimental data for RNA constructs are not yet available, model calculations indicate no obvious stereochemical hindrances. Clearly, secondary and tertiary interactions in rRNA, tRNA, transcripts, and in viruses with a single stranded genome are suitable circumstances in which the parallel stranded helical orientation could provide additional stabilization or specificity, particularly if proteins intervene. In fact, single *trans* base pairs are observed in tRNA crystal structures (24,25).

### *Acknowledgments*

We thank Gudrun Heim for technical assistance. One of us (T. M. J.) is indebted to N. Pattabiraman for drawing his attention to ps-DNA in 1985.

#### *References and Footnotes*

1. Pattabiraman, N., *Biopolymers 25*, 1603-1606 (1986).
2. van de Sande, J.H., Ramsing, N.B., Germann, M.W., Elhorst, W., Kalisch, B.W., von Kitzing, E., Pon, R.T., Clegg, R.M. and Jovin, T.M., *Science 241*, 551-557 (1988).
3. Ramsing, N.B. and Jovin, T.M., *Nucleic Acids Res. 16*, 6659-6676 (1988).
4. Germann, M.W., Kalish B.W. and van de Sande, J.H., *Biochemistry 27*, 8302-8306 (1988).
5. Rippe, K., Ramsing, N.B. and Jovin, T.M., *Biochemistry*, in press (1989).
6. Ramsing, N.B., Rippe, K. and Jovin, T.M., *Biochemistry*, in press (1989).
7. Rippe, K. and Jovin, T.M., *Biochemistry*, in press (1989).
8. Rippe, K., Ramsing, N.B., Klement, R. and Jovin, T.M., submitted (1989).
9. Gorenstein, D.G., Schroeder, S.A., Fu, J.M., Metz, J.T., Roongta, V. and Jones, C.R., *Biochemistry 27*, 7223-7237 (1988).
10. Teng, M., Usman, N., Frederick, C.A. and Wang, A.H.-J., *Nucleic Acids Res. 16*, 2671-2690 (1988).
11. Pjura, P.E., Grzeskowiak, K. and Dickerson, R.E., *J. Mol. Biol. 197*, 257- 271 (1987).
12. Larsen, T.A., Goodsell, D.S., Cascio, D., Grzeskowiak, K. and Dickerson, R.E., in *J. Biomol. Struct. Dyn. 7*, 477-491 (1989).
13. Jovin, T.M., McIntosh, L.P., Arndt -Jovin, D.J., Zarling, D.A., Robert-Nicoud, M., van de Sande, J.H., Jorgensen, K.F. and Eckstein, F., *J. Biomol. Struct Dynam. 1*, 21-57.
14. Jovin, T.M., Soumpasis, D.M. and McIntosh, L.P., *Ann. Rev. Phys. Chem. 38*, 521-560 (1987).
15. Pohl, F.M., Jovin, T.M., Baehr, W. and Holbrook, J.J., *Proc. Natl. Acad. Sci. USA 69*, 3805-3809 (1972).
16. Stryer, A., *Ann. Rev. Biochem. 47*, 819-846 (1978).

17. Cardullo, R.A., Agrawal, S., Flores, C., Zamecnik, P.C. and Wolf, D.E., *Proc. Natl. Acad. Sci. USA 85*, 8790-8794 (1988).
18. Duckett, D.R., Murchie, A.I.H., Clegg, R.M., von Kitzing, E., Diekmann, S. and Lilley, D.M.J., *Structure & Methods, Volume 1: Human Genome Initiative & DNA Recombination*, (Eds., R.H. Sarma and M.H. Sarma) Adenine Press (1990).
19. Chan, S.S., Arndt-Jovin, D.J. and Jovin, T.M., *J. Histochem Cytochem. 27*, 56-54 (1979).
20. Campbell, V.W. and Jackson, D.A., *J. Biol. Chem. 255*, 3726-3735 (1980).
21. Wu, C., *Nature 317*, 84-87 (1985).
22. Suck, D., Lahm, A. and Oefner, C., *Nature 332*, 464-468 (1988).
23. Drew, H.R. and Travers, A.A., *Nucleic Acids Res. 13*, 4445-4467 (1985).
24. Kim, S.H., Sussman, J.L., Suddath, F.L., Quigley, G.J., McPherson, A., Wang, A.H.J., Seeman, N.C. and Rich, A., *Proc. Natl. Acad. Sci. USA 71*, 4970-4974 (1974).
25. Westhof, E. Dumas, P. and Moras, D., *J. Mol. Biol. 184*, 119-145 (1985).
26. Klement, R., Soumpasis, D.M. and Jovin, T.M., *Biopolymers*, in press.